Supporting Information

Redox-active radical as an effective nanoelectronic component: stability and electrochemical tunnelling spectroscopy in ionic liquids

Alexander V. Rudnev,[a,b] Carlos Franco,[c] Núria Crivillers,[c] Gonca Seber,[c] Andrea Droghetti,[d] Ivan Rungger,[e] Ilya V Pobelov,[a] Jaume Veciana,[c] Marta Mas-Torrent,[c] Concepció Rovira[c]

[a] University of Bern, Department of Chemistry and Biochemistry, Freiestrasse 3, 3012 Bern, Switzerland
[b] Russian academy of sciences A.N. Frumkin Institute of Physical chemistry and Electrochemistry RAS, Leninskii pr. 31, Moscow, 119991, Russia
[c] Department of Molecular Nanoscience and Organic Materials, Institut de Ciència de Materials de Barcelona (ICMAB- CSIC) and CIBER-BBN, Campus la Universitat Autonoma Barcelona (UAB), 08193 Bellaterra, Spain
[d] Nano-Bio Spectroscopy Group and European Theoretical Spectroscopy Facility (ETSF), Universidad del Pais Vasco CFM, CSIC-UPV/EHU-MPC & DIPC, Avenida Tolosa 72, 20018 San Sebastian, Spain.
[e] Materials Division, National Physical Laboratory, Teddington, TW11 0LW, United Kingdom

Experimental details

Surface modification of the flame-annealed Au(1 1 1) electrodes was carried out according to the following protocol: PTM-C8-SH (Figure 1 in the main text) and αH-PTM-C8-SH (Scheme S1) SAMs were deposited on Au(1 1 1) by immersing a freshly prepared electrode in 0.3 mM solutions of the PTM derivatives in toluene (HPLC) at the temperature of 40 °C for 24 h. The samples were removed from the solution after incubation, rinsed with dichloromethane (DCM, HPLC), dried in a stream of argon, and subsequently transferred into the electrochemical or STM cell.

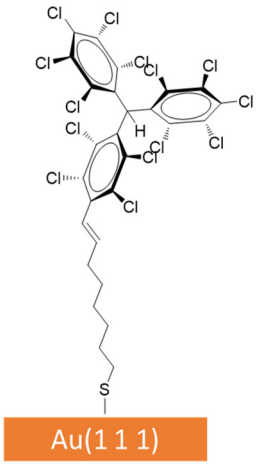

Scheme S1. αH-PTM-C8-SH SAM on Au(1 1 1)

As electrolytes we employed different ionic liquids: names, abbreviations, source and quality are given in Table S1. The ILs were used without additional purification. Before STM and final voltammetric experiments, the molecular sieves (3 Å, Merck) were added directly into respective cells with an IL to dry it. Before use, the molecular sieves were thoroughly cleaned with absolute ethanol and Milli-Q water (18.2 MΩ, 2 ppb TOC) and activated for at least 7 days at 200ºC. In some experiments we used trimethylamine (Et_3N, Sigma Aldrich, ≥99.5%) as an additive.

Furthermore, we used an electrolyte solution prepared from tetrabutylammonium hexafluorophosphate n-Bu_4NPF_6 in acetonitrile (Fisher Chemical, HPLC). The glassware and plastic parts were cleaned in piranha solution or boiling in 25% nitric acid followed by cooking and extended rinsing with Milli-Q water and overnight drying in an oven at 105°C.

A Clavillier-type Au(1 1 1) bead single crystal electrode with an oriented and polished surface (area 0.030 cm^2) served as a working electrode in the electrochemical studies. For in situ STM/STS experiments we used a disk Au(1 1 1) electrode of 10 mm diameter. Contact of the working electrode with the electrolyte was established under strict potential control. A platinum wires served as counter and quasi-reference electrodes in both electrochemical and STM studies.

The macroscopic electrochemical measurements in ionic liquids were performed in a dedicated all-glass cell employing an Autolab PGSTAT30 potentiostat. The STM/STS measurements were carried out with a PicoSPM system (Molecular Imaging) in a sealed, argon-filled chamber. The controlled environment ensures the long-term stability of the PTM radicals. The STM liquid cell was mounted on top of the Au(1 1 1) electrode via an O-ring (Kalrez). The STM tips were electrochemically etched gold wires (0.25 mm diameter) coated with polyethylene.

In situ STS measurements were carried out employing "electrolyte gating".[1] The potentials of both working electrodes (E_S and E_T for modified Au(1 1 1) substrate and coated gold tip, respectively) were swept simultaneously (with a constant bias voltage $E_{bias} = E_T - E_S$). Constant bias mode STS curves (I_t vs. E_S) were recorded at a fixed geometry of the tunneling junction with the feedback being temporarily switched off. First, the STM tip was brought into tunneling gap over PTM-C8-SH SAM with a preset current $I_{SetPoint}$ and bias E_{bias}, then the feedback was switched off and an STS curve is recorded. Afterwards, the feedback was switched on for a second to stabilize the junction, and further this cycle was repeated again. The data were collected automatically with a lab-written Visual Basic Script, which controlled the STM setup. The tip was repositioned after each 25 sweeps to a new area to ensure a better statistics. Usually around 200 spectra were recorded for each set of conditions. The data are presented as 2D histograms, which were constructed based on a LabVIEW program written by Dr. Artem Mishchenko. The following algorithm was applied: individual IV traces were first binned in 2D space (usually 200×200 bins) and the resulting individual 2D histograms were summed up. The results, plotted as intensity graphs, represent statistically significant in situ STS data. All electrochemical and *in situ* STM/STS experiments were performed under argon (5N) atmosphere at room temperature (295 K).

EPR spectra were recorded in a Bruker ELEXYS E500 X-band spectrometer. UV-Vis spectra were recorded on a Varian Carey 5000 in double-beam mode. The manipulation of the radicals in solution was performed under red light.

Characterization of PTM-C8-SH adlayers on Au(1 1 1) electrodes.

The CVs of the freshly prepared PTM-C8-SH SAM are shown in Figure S1a. CV results in acetonitrile and 0.1 M *n*-Bu_4NPF_6 as electrolyte (using silver wire as a reference electrode) showed one reversible pair of redox peaks with a formal potential $E_{1/2}$ of -0.08 V (vs. Ag) and a peak-to-peak separation ΔE = 27 mV at a scan rate of 1 Vs^{-1}. Start potential was 0.2 V, at which the radical form of PTM is stable. Cathodic (negative currents) and anodic (positive currents) peaks are assigned to the reduction of PTM radical moieties to anions and the reverse oxidation of the anions to the radicals, respectively. A small peak-to-peak separation and the linear dependence of peak heights on scan rate (top inset) indicate that the redox process is surface-confined. The redox signal was rather stable as tested by multiple potential cycling, during which no noticeable changes in CVs were detected (bottom inset). Electrochemical experiments in organic solvents were performed with a potensiostat/galvanostat Autolab/PGSTAT204 from Metrohm Autolab B.V. in a standard three-electrode cell.

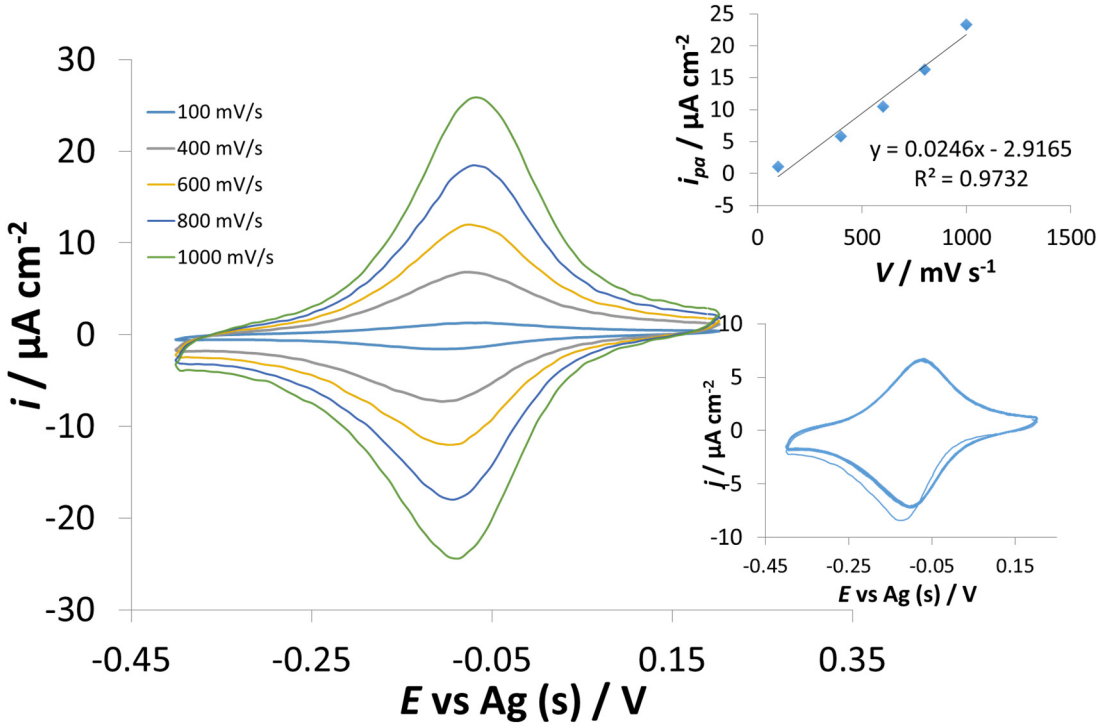

Figure S1. CVs of the radical PTM-C8-SH SAM in 0.1 M solution of *n*-Bu_4NPF_6 in acetonitrile, recorded at different scan rates. Top inset: Plot of the peak current *vs* scan rate. Bottom inset: Potential cycling (20cycles) at 0.4 Vs^{-1}.

Table S1. The list of different ionic liquids, in which PTM-C8-SH adlayer was tested. The stability time was estimated as a time of continuous potential cycling until the redox charge under peaks decreased to 10% of the initial value.

Abbreviation	Source and quality	Name	Structure	Stability
[Emim][Tf_2N]	Merck, for synthesis, ≥98.0%	1-ethyl-3-methylimidazolium bis(trifluoromethylsulfonyl)imide	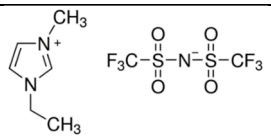	< 10 min
[Emim][$EtSO_4$]	Alfa Aesar, 99%	1-ethyl-3-methylimidazolium ethyl sulfate	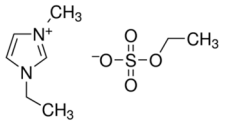	~10 min
[Bmim][BF_4]	Sigma Aldrich, HPLC, ≥97.0%	1-Butyl-3-methylimidazolium tetrafluoroborate	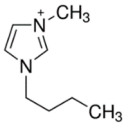	< 10 min
[Bmim][DCA]	Merck, for synthesis, ≥98.0%	1-Butyl-3-methylimidazolium dicyanamide	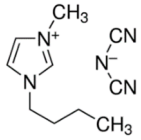	< 10 min
[Bmim][TfO]	Merck, high purity, ≥99.0%	1-butyl-3-methylimidazolium trifluoromethanesulfonate	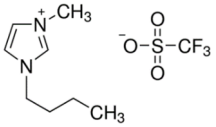	< 10 min
[Hmim][PF_6]	Fluka, ≥97.0%	1-Hexyl-3-methylimidazolium hexafluorophosphate	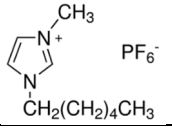	< 10 min
[BMP][Tf_2N]	Merck, high purity, ≥99.0%	1-butyl-1-methylpyrrolidinium bis(trifluoromethylsulfonyl)imide	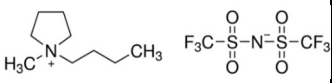	~ 30-60 min
[SEt_3][Tf_2N]	Fluka, for electrochem. ≥99.0%	Triethylsulfonium bis(trifluoromethylsulfonyl)imide	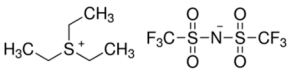	~30-60 min

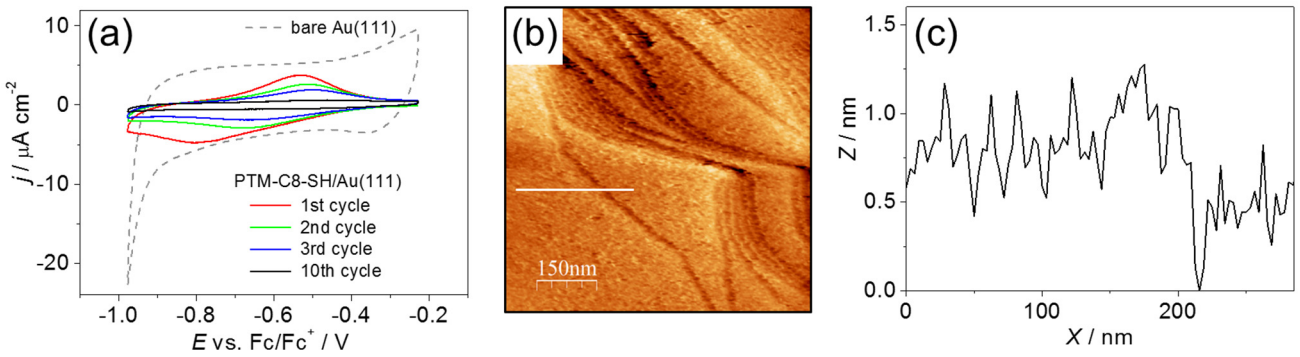

Figure S2. (a) Consecutive CVs of PTM-C8-SH/Au(111) in [Emim][$EtSO_4$]. The numbers of some cycles are indicated. Scan rate is 0.05 V s^{-1}. (b) A representative in situ STM image of PTM-C8-SH/Au(111). E_S = -0.20 V (vs. Pt), E_{bias} = 0.1 V, $I_{SetPoint}$ = 25 pA. (c) Cross-section along white line in the panel (b).

The mechanism of anion protonation in ILs is not clear. However, the following explanations can be proposed. With ILs containing imidazolium-based cations ([Emim], [Bmim], and [Hmim]) we observed a fast degradation of redox signal independently on the anion (Table S1). On the other hand, utilization of ILs with [BMP] and [SEt_3] cations led to a better stability of the PTM anion. It was reported that the slightly acidic C2 proton in the dialkyl imidazolium ring produces certain acid catalysis effects.[2] Furthermore, it seems that PTM anion displays strong proton-acceptor properties. Therefore, PTM anion can accept the C2 proton from an imidazolium-based cation and form the stable redox-nonactive αH-PTM moiety. This reaction is assisted by electrostatic interaction between the PTM anion and the dialkyl imidazolium cation. However, we notice that the protonation of PTM anion was also observed in dialkyl-imidazolium-free ionic liquids such as [BMP][Tf_2N] and [SEt_3][Tf_2N] (Table S1), although the degradation occurred proceeded slower. Furthermore, residual water may also serve as a source of protons for this reaction.

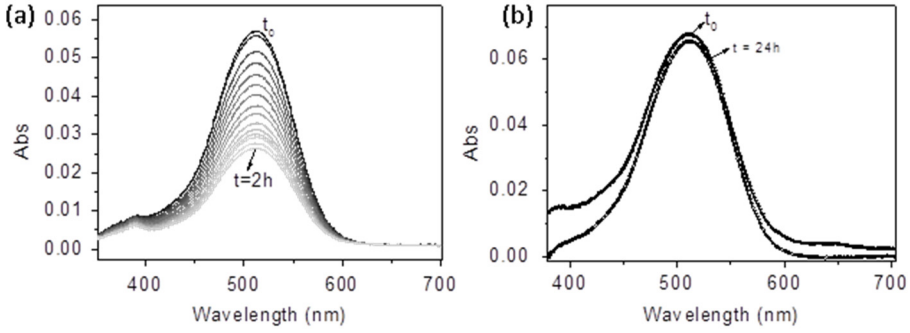

Figure S3. Evolution of the UV/Vis spectrum of $PTM^{-}K^{+}$ [18-Crown-6] with time in (a) [Emim][$EtSO_4$] and (b) [Emim][$EtSO_4$] + Et_3N (15:1 v/v).

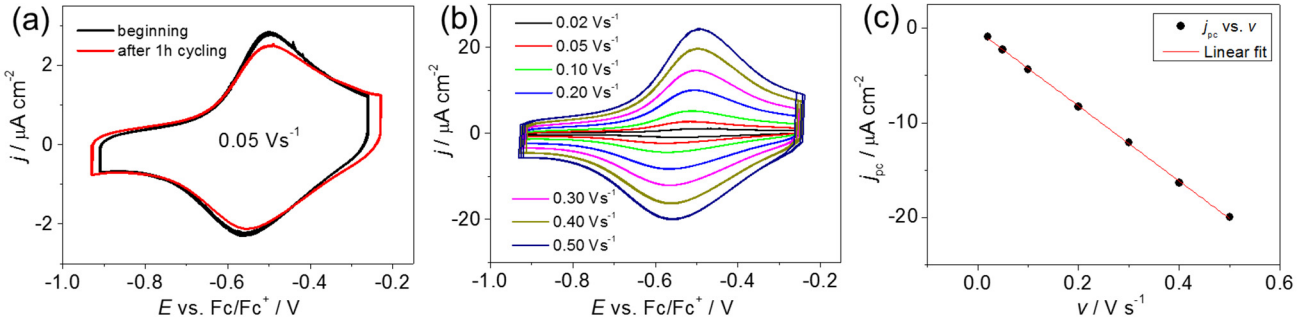

Figure S4. (a) Cyclic voltammograms of radical PTM-C8-SH/Au(111) in [Emim][$EtSO_4$] + Et_3N (15:1 v/v) with molecular sieves: at the beginning of the experiment and after 1 h of potential cycling. (b) CVs at different scan rates. (c) Plot of the cathodic current peak height vs. the scan rate and the linear fit.

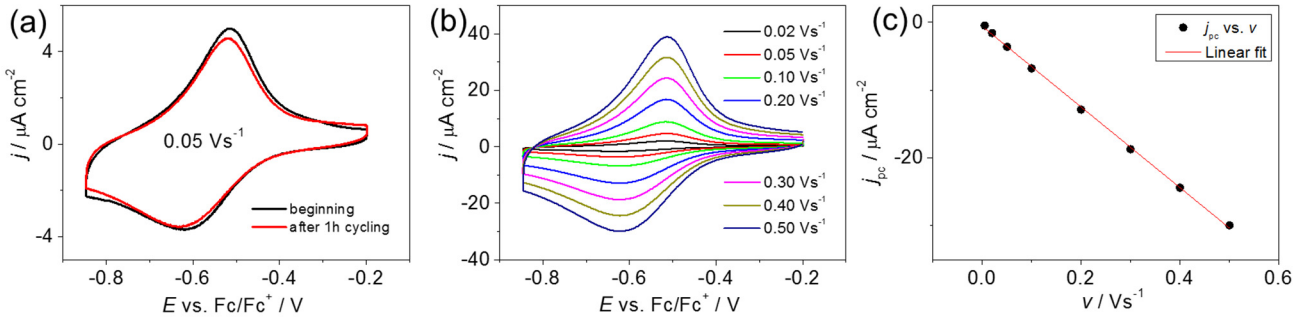

Figure S5. (a) Cyclic voltammograms of radical PTM-C8-SH/Au(111) in [SEt_3][Tf_2N] + Et_3N (15:1 v/v) with molecular sieves: at the beginning of the experiment and after 1 h of potential cycling. (b) CVs at different scan rates. (c) Plot of the cathodic current peak height vs. the scan rate and the linear fit.

The CV measurements in [Emim][$EtSO_4$] and [SEt_3][Tf_2N] ILs with addition of Et_3N demonstrated a high stability of voltammetric redox peaks. Examples are shown in Figures S4 and S5. CV shape does not change considerably even after cycling for 1 h, and linear dependence of peak height vs. scan rate indicates surface-confined redox process. We notice that usage of molecular sieves (added directly into the cell) also improves the redox-stability of the PTM-alkyl-SH SAM.

In situ STM images of PTM-C8-SH/Au(111) in [Emim][$EtSO_4$] + Et_3N (Figure S6) demonstrate that the SAM is compact, but disordered. Similar images were obtained in the [SEt_3][Tf_2N] ionic liquid (Figure 2 in the manuscript).

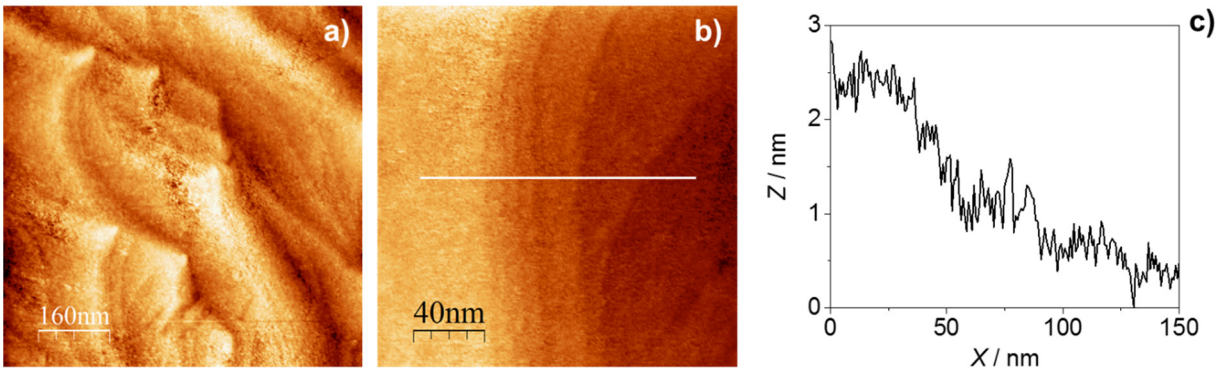

Figure S6. (a,b) *In situ* STM images of radical PTM-C8-SH/Au(111) in [Emim][$EtSO_4$] + Et_3N (15:1 v/v) with molecular sieves. E_S = -0.3 V, E_T = -0.2 V, $I_{SetPoint}$ = 0.06 nA. (c) Cross-section along the white line in the panel (b).

Estimation of maximal packing of PTM-C8-SH on Au(1 1 1)

The theoretical maximum of PTM-C8-SH coverage was estimated as follows. The bulky PTM moiety has a planar triangular shape. Hence, the closely-packed molecules attached vertically can be represented as rectangular parallelepipeds with the base edges 1.3 nm and 0.78 nm and projected area 1.014 nm^2 as depicted in Figure S7. Therefore, the maximal coverage is $9.86 \cdot 10^{13}$ molecules per cm^2, or $1.64 \cdot 10^{-10}$ mol cm^{-2}.

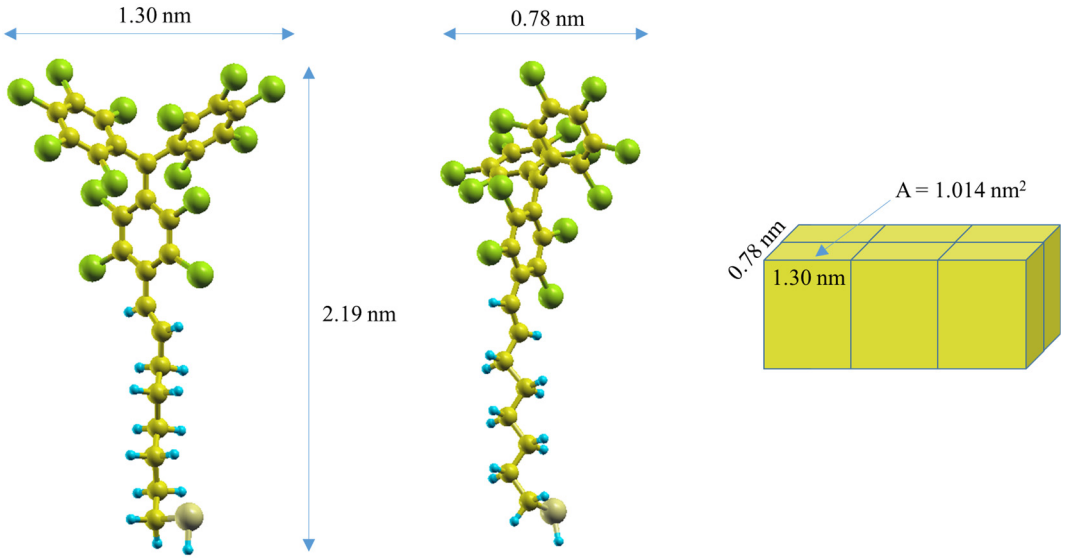

Figure S7. The representation of the closest packed adlayer of the PTM-C8-SH molecules as rectangular parallelepipeds with respective dimensions. The area of one molecule projected on a substrate is indicated in the figure.

Assuming the molecules lie on the surface as depicted in the left picture of Figure S7 (top view), one can suggest that the molecules have a triangular projection shape with the base of 13.0 Å and height of 21.9 Å. Then the area of such a triangle will be 1.424 nm^2, giving a maximal coverage 7.02 10^{13} molecules per cm^2, or 1.17 10^{-10} mol cm^{-2}. However, such a coverage suggests

the very uniform arrangement of PTM triangles. More realistically they are oriented randomly and since the molecule is very long (21.9 Å), the coverage would decrease significantly. The arrangement of molecules on the Au(1 1 1) surface is difficult to deduce from our STM results, but relying on the coverage values of 1.1-1.2 10^{-10} mol cm^{-2} as obtained from CVs, we propose that the majority of the molecules are adsorbed in vertical-tilted configuration.

Redox-mediated electron tunneling (RMET): Kuznetsov-Ulstrup model.[3]

Several experimental works demonstrated a redox-mediated electron transfer (RMET)[3] trough different redox-active organic molecules,[1, 4-7] metal-organic complexes[8, 9] and biomolecules[10, 11] adsorbed on an electrode surface as well as through single molecule junction.[12, 13] Kuznetsov and Ulstrup treated the RMET process as a sequence of oxidation and reduction events occurring when the effective potential of the redox center lies between the potentials of two adjacent electrodes (a KU model), such as the tip of a STM (E_T) and the corresponding substrate (E_S). Assuming a strong electronic coupling between the molecule and both adjacent electrodes (adiabatic limit), we also rationalize RMET in our case by KU model, two-step electron transfer with partial vibrational relaxation. For further details we refer to previous reports.[1, 7, 13]

The master curve in Figure 4c was fitted by using a numerical expression[1, 9, 13] (1) for the enhanced tunneling current obtained in the frameworks of the KU model. The fitting parameters for the curve in Figure 4c are given in Table S2 (E_{bias} = 0.1 V and $I_{SetPoint}$ = 0.1 nA).

$$I_{enh} = 1820E_{bias}\left\{exp\left[\frac{9.73}{\lambda}(\lambda + \xi\eta + \gamma E_{bias})^2\right] + exp\left[\frac{9.73}{\lambda}(\lambda + E_{bias} - \xi\eta - \gamma E_{bias})^2\right]\right\}^{-1} \quad (1)$$

Here, I_{enh} is enhanced tunneling current during constant-bias STS (in nA); bias voltage (in V) $E_{bias} = (E_T - E_S)$ and overpotential (in V) $\eta = (E_S - E_0)$, where E^0 is the equilibrium potential for the electrochemical oxidation-reduction of a particular species; λ is reorganization energy (eV). ξ and γ, both ranging between 0 and 1, are model parameters describing the shift of η_{eff} with the variation of η and E_{bias}, respectively.

$$\eta_{eff}=(E_{eff}-E^0)=\xi\eta+\gamma_{Ebias}=(\xi-\gamma)\cdot\eta+\gamma\cdot\eta_T \quad (2)$$

The expression for the effective overpotential can be reformulated as a sum of the fractions of the sample overpotential η and of the tip overpotential $\eta_T = (E_T - E^0)$.[7]

Table S2. Model parameters obtained by fitting eq. 1 to the curve shown in Figure 3c in the main text.

λ / eV	ξ	γ
0.39	0.57	0.57

Calculation of the inner-sphere reorganization energy

The inner-sphere reorganization energy of the molecule[15] when going from neutral to the anion state, $\lambda_{i,an}$, is defined as the difference between the energy of the anion at the relaxed atomic structure of the neutral state, E_{an}, and the energy of the anion at its relaxed structure, E_a, so that $\lambda_{i,an}=E_{an} - E_a$. The reorganization energy for the reverse transition from anion to neutral state, $\lambda_{i,na}$, is given by $\lambda_{i,na}=E_{na} - E_n$, where E_{na} is the energy of the neutral system at the anion relaxed geometry, and E_n is the energy of the neutral state at its relaxed geometry. Since usually for small deformations $\lambda_{i,an} \approx \lambda_{i,na}$, we can determine the average inner-sphere reorganization energy of a single molecule for both processes as $\lambda_i =(\lambda_{i,an} + \lambda_{i,na})/2$. These energies and atomic structures were calculated for the gas-phase PTM molecule by density functional theory (DFT) using the all-electron code FHI-AIMS[16]. The Perdew–Burke–Ernzerhof (PBE)[17,18] generalized gradient approximation to the exchange-correlation density functional was used together with numerical atom centered basis, where the free-atom-like radial orbitals are improved by adding further radial functions grouped in the tier 2 set. This corresponds to the pre-constructed "tight" default setting. Geometry optimization were performed until the ionic forces were smaller than 0.01 eV/Ang. The calculated values are then $\lambda_{i,an}$ = 0.082 eV, and $\lambda_{i,na}$ = 0.077 eV. These are indeed similar, and the average value is then λ_i = 0.080 eV.

We would like to compare the reorganization energy of PTM with that for perylene bisimide-type molecule, which also demonstrated RMET in STS configuration.[14] For this reason, we calculate the λ_i for perylene bisimide derivative (Scheme S2) in the same way as for PTM. The average value is λ_i = 0.097 eV.

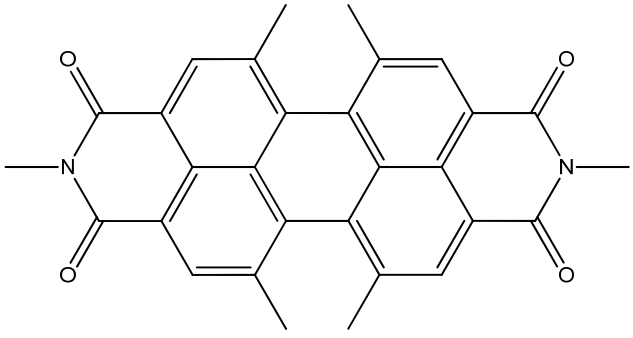

Scheme S2. Structure of perylene bisimide derivative used for the calculations of inner-sphere reorganization energy.

References

1. I. V. Pobelov, Z. H. Li and T. Wandlowski, *J. Am. Chem. Soc.*, 2008, **130**, 16045-16054.
2. D. R. MacFarlane, J. M. Pringle, K. M. Johansson, S. A. Forsyth and M. Forsyth, *Chem. Commun.*, 2006, 1905-1917.
3. J. Zhang, A. M. Kuznetsov, I. G. Medvedev, Q. Chi, T. Albrecht, P. S. Jensen and J. Ulstrup, *Chem. Rev.*, 2008, **108**, 2737-2791.
4. N. J. Tao, *Phys. Rev. Lett.*, 1996, **76**, 4066-4069.
5. P. Salvatore, A. Glargaard Hansen, K. Moth-Poulsen, T. Bjornholm, R. John Nichols and J. Ulstrup, *Phys. Chem. Chem. Phys.*, 2011, **13**, 14394-14403.
6. Z. Li, Y. Liu, S. F. L. Mertens, I. V. Pobelov and T. Wandlowski, *J. Am. Chem. Soc.*, 2010, **132**, 8187-8193.
7. A. V. Rudnev, I. V. Pobelov and T. Wandlowski, *J. Electroanal. Chem.*, 2011, **660**, 302-308.
8. T. Albrecht, K. Moth-Poulsen, J. B. Christensen, J. Hjelm, T. Bjørnholm and J. Ulstrup, *J. Am. Chem. Soc.*, 2006, **128**, 6574-6575.
9. T. Albrecht, A. Guckian, J. Ulstrup and J. G. Vos, *Nanotechnology, IEEE Transactions on*, 2005, **4**, 430-434.
10. J. Zhang, Q. Chi, A. G. Hansen, P. S. Jensen, P. Salvatore and J. Ulstrup, *FEBS Lett.*, 2012, **586**, 526-535.
11. J. Zhang, Q. Chi, A. M. Kuznetsov, A. G. Hansen, H. Wackerbarth, H. E. M. Christensen, J. E. T. Andersen and J. Ulstrup, *J. Phys. Chem. B*, 2002, **106**, 1131-1152.
12. H. M. Osorio, S. Catarelli, P. Cea, J. B. G. Gluyas, F. Hartl, S. J. Higgins, E. Leary, P. J. Low, S. Martín, R. J. Nichols, J. Tory, J. Ulstrup, A. Vezzoli, D. C. Milan and Q. Zeng, *J. Am. Chem. Soc.*, 2015, **137**, 14319-14328.
13. N. J. Kay, S. J. Higgins, J. O. Jeppesen, E. Leary, J. Lycoops, J. Ulstrup and R. J. Nichols, *J. Am. Chem. Soc.*, 2012, **134**, 16817-16826.
14. C. Li, A. Mishchenko, Z. Li, I. Pobelov, W. Th, X. Q. Li, F. Würthner, A. Bagrets and F. Evers, *J. Phys.: Condens. Matter*, 2008, **20**, 374122.
15. S. F. Nelsen, S. C. Blackstock and Y. Kim, *J. Am. Chem. Soc.*, 1987, **109**, 677-682.
16. V. Blum, R. Gehrke, F. Hanke, P. Havu, V. Havu, X. Ren, K. Reuter and M. Scheffler, *Comput. Phys. Commun.*, 2009, **180**, 2175-2196.
17. J. P. Perdew, K. Burke and M. Ernzerhof, *Phys. Rev. Lett.*, 1996, **77**, 3865-3868.
18. J. P. Perdew, K. Burke and M. Ernzerhof, *Phys. Rev. Lett.*, 1997, **78**, 1396.